Title: Overexpressing the hydroxycarboxylic acid receptor 1 in mouse brown adipose tissue restores glucose tolerance and insulin sensitivity in diet-induced obese mice.

Authors

Hyeon-Young Min[1,2‡], Jiyeon Hwang[1,2‡], Yuna Choi[1,2], and Young-Hwan Jo[1,2,3]*

Affiliations

[1]The Fleischer Institute for Diabetes and Metabolism

[2]Division of Endocrinology, Department of Medicine

[3]Department of Molecular Pharmacology, Albert Einstein College of Medicine, NY, USA

[‡] Both authors contributed equally to this work.

*** Corresponding author: young-hwan.jo@einsteinmed.edu**

Departments of Medicine and Molecular Pharmacology

Albert Einstein College of Medicine,

1300 Morris Park Ave, Bronx, NY 10461

Tel: 718-430-3495

Abstract:

Interscapular BAT (BAT) plays an important role in controlling glucose homeostasis. Increased glucose entry and glycolysis in BAT result in lactate production and release. The adipose tissue expresses the lactate receptor hydrocarboxylic acid receptor 1 (HCAR1), markedly downregulated in male diet-induced obese (DIO) and *ob/ob* mice. In this study, we examined the role of HCAR1 in BAT in controlling glucose homeostasis in male DIO mice. We overexpressed HCAR1 in BAT by injecting adeno-associated viruses (AAV) expressing HCAR1 into the BAT pads of male DIO C57BL/6J mice. Overexpressing HCAR1 in BAT resulted in augmented glucose uptake by BAT in response to treatment with the HCAR1 agonist. HCAR1 overexpression elevated BAT temperature associated with increased thermogenic gene expression in BAT. HCAR1 overexpression prevented body weight gain in male DIO mice. Importantly, mice overexpressing HCAR1 in BAT exhibited improved glucose tolerance and insulin sensitivity. HCAR1 overexpression upregulated the *Slc2a4* gene expression and promoted GLUT4 trafficking to the plasma membrane. In addition, mice overexpressing HCAR1 displayed a decrease in HSL phosphorylation and increased lipogenic enzyme gene expression in BAT. Unlike DIO mice, overexpressing HCAR1 in BAT of mice fed a low-fat diet did not change body weight gain and glucose homeostasis. Taken together, our results support the interpretation that HCAR1 expressed in BAT promotes glucose entry and reduces lipolysis in BAT of male DIO mice. As activation of HCAR1 in BAT restores body weight, glucose tolerance, and insulin sensitivity in male DIO mice, targeting HCAR1 in BAT would provide an alternative way to control body weight and euglycemia in individuals with obesity.

New and Noteworthy: HCAR1 expressed in BAT can promote glucose entry and reduce lipolysis, resulting in body weight loss and increased insulin sensitivity. Hence, targeting HCAR1 in BAT would provide an alternative way to control body weight and euglycemia in individuals with obesity.

50 **Introduction**

51 Stimulation of brown adipose tissue (BAT) regulates whole-body triglyceride clearance, glucose
52 disposal, insulin sensitivity, and energy expenditure in humans (1-7). Hence, this organ is considered an
53 important therapeutic target against obesity and diabetes in humans, although BAT represents only
54 a small fraction of body mass. While BAT takes up circulating glucose that can be used to generate heat
55 in humans and rodents (8-13), the contribution of glucose to heat production in BAT remains
56 controversial (14-16). Early studies show that lactate production accounts for a large proportion of
57 insulin- and norepinephrine-induced glucose uptake by BAT (17, 18). In line with these early findings,
58 cold- and β3-adrenergic receptor (β3AR)-induced activation of interscapular BAT (BAT) in mice
59 upregulates mRNA and protein expression of the lactate dehydrogenase (LDH)-A that preferentially
60 catalyzes pyruvate conversion to lactate (11, 19). This upregulation leads to a significant release of lactate
61 from BAT in rodents (18, 20). Notably, a recent human study by the Stimson research group demonstrates
62 that BAT produces and releases lactate in response to glucose entry during warm conditions (7). Hence, it
63 is necessary to better understand the physiological role of lactate in the control of glucose and lipid
64 metabolism in BAT.

65 We previously demonstrated that optogenetic stimulation of sympathetic nerves of BAT
66 promoted nonshivering thermogenesis and glucose uptake by BAT in mice (11). In the presence of the
67 LDH inhibitor, however, optogenetic stimulation of sympathetic nerves of BAT failed to increase BAT
68 temperature and lower blood glucose levels, suggesting that LDH activity appears to be essential for the
69 acute activation of BAT thermogenesis (11). BAT expresses the monocarboxylate transporter 1 (MCT1)
70 that catalyzes the rapid transport of monocarboxylates such as lactate, pyruvate, and ketone bodies in the
71 mitochondrial and plasma membrane (11, 21, 22). Increased sympathetic tone to BAT upregulates
72 expression of the *Mct1* mRNA (11). The genetic and pharmacological blockade of MCT1 inhibits the
73 acute effect of optogenetic stimulation of sympathetic nerves of BAT on BAT thermogenesis and glucose
74 uptake (11). These prior findings suggest that intracellular glycolysis and lactate production in BAT are
75 important and required for the adrenergic activation of nonshivering thermogenesis.

76 In addition to its role as fuel, it has been shown that lactate acts as a signaling molecule with
77 autocrine-, paracrine-, and endocrine-like effects in the white adipose tissue (WAT) (23, 24). In fact,
78 MCT1 can bidirectionally transport lactate across the plasma membrane (22). Of particular interest is that
79 the lactate receptor hydrocarboxylic acid receptor 1 (HCAR1) is primarily expressed in white and brown
80 adipocytes in both rodents and humans (23, 25, 26). Activating HCAR1 by lactate inhibits lipolysis and
81 loss of the *Hcar1* gene impairs the antilipolytic effect in the adipose tissue (25). Additionally, HCAR1
82 signaling improves insulin-mediated anti-lipolysis in white adipocytes (23). We previously showed that
83 male DIO C57BL/6J mice exhibited a significant reduction in HCAR1 expression in BAT (27), consistent

84 with prior studies showing that male DIO and *ob/ob* mice display decreased *Hcar1* gene expression in the
85 adipose tissue (28, 29). Hence, disrupted HCAR1 action in the adipose tissue could contribute to insulin
86 resistance and metabolic dysfunction in obese animals.
87 In this study, we examined the role of HCAR1 in BAT in controlling glucose homeostasis in male
88 DIO mice. Specifically, we overexpressed HCAR1 in BAT of male DIO C57BL/6J mice. HCAR1
89 overexpression in BAT significantly increased BAT temperature. Importantly, mice overexpressing
90 HCAR1 in BAT were protected against DIO and exhibited improved glucose and insulin tolerance.
91
92 **Material and Methods**
93 **Ethics statement**
94 All mouse care and experimental procedures were approved by the Institutional Animal Care
95 Research Advisory Committee of the Albert Einstein College of Medicine and were performed in
96 accordance with the guidelines described in the NIH guide for the care and use of laboratory animals.
97 Viral injections were performed under isoflurane anesthesia.
98 **Animals**
99 9-weeks old male DIO C57BL/6J (JAX stock # 380050, IMSR_JAX:380050) were purchased
100 from the Jackson Laboratory and fed a high-fat diet (HFD; Research Diets Cat#D12492; 20% calories by
101 carbohydrate, 20% by protein, and 60% by fat). To determine if the effect of HCAR1 is coupled with
102 changes in nutrient availability, 9-weeks old male C57BL/6J mice were fed a low-fat diet (LFD; Research
103 Diets Cat#D12492J; 70% calories provided by carbohydrates, 20% by protein, and 10% by fat). Age-
104 matched male mice were randomly assigned to experimental groups. Mice were housed in cages under
105 conditions of controlled temperature (22 °C) with a 12:12 hr light-dark cycle and water provided *ad*
106 *libitum*. Mice were euthanized by an overdose of isoflurane at the end of the experiments.
107 **Viral injections into BAT**
108 10-weeks old mice were anesthetized deeply with 3% isoflurane. A deep level of anesthesia was
109 maintained throughout the surgical procedure. Under isoflurane anesthesia (2%), AAV5-CMV-HCAR1-
110 GFP (Applied Biological Materials, Inc, titer, 4.69 X 10^{12} GC/ml) and AAV5-CAG-GFP (Addgene
111 Cat#37825-AAV5, titer, 4.3 X 10^{12} GC/ml) viruses were bilaterally injected into the BAT pads of male
112 C57BL/6J mice using a Hamilton syringe (4 µl per pad). At the end of the experiments, the expression of
113 viral transgenes was confirmed by performing an RT-qPCR analysis of *Hcar1* in BAT. When the viral
114 injections missed the BAT pads, we excluded data. The experiment assignment was *blinded* to
115 investigators who participated in viral injection, experiments, and data analyses.
116 **Measurement of BAT temperature**

117 To directly measure BAT temperature, we implanted a miniature radio frequency identification
118 (RFID) transponder with an integrated temperature biosensor (size, 2.1mm x 13mm, temperature
119 accuracy, ±0.1ºC at 38ºC, Unified Information Devices (UID), Inc) just underneath the BAT pads
120 immediately after viral injections. Each cage containing 4 mice was placed on a mouse matrix plate (UID,
121 Inc) and the temperature data were collected every 5 s with Mouse Matrix software (version 1.1) and
122 stored on a PC.

123 **Measurement of body weight and blood glucose levels**

124 Body weight was measured weekly at 9 am. Body composition for fat mass and fat-free mass
125 were assessed by ECHO MRI at our animal physiology core. Blood samples were collected from the
126 mouse tail, and a small drop of blood was placed on the test strip of a glucose meter. Non-fasting basal
127 glucose levels were measured at 9:00 am. Fasting blood glucose levels were measured after an overnight
128 fast once at 10 weeks post viral injection.

129 **Assessment of energy expenditure and locomotor activity**

130 Mice were individually housed in the calorimeter cages and acclimated to the respiratory
131 chambers for at least 2 days prior to gas exchange measurements. Indirect calorimetry was performed for
132 5 days at the end of 10 weeks on high-fat feeding using an open-circuit calorimetry system. O_2
133 consumption and CO_2 production were measured for each mouse at 10-min intervals over a 24-h period.
134 Energy expenditure was calculated based on O_2 consumption, CO_2 consumption and body mass. All data
135 were analyzed with a Web-based Analysis Tool for Indirect Calorimetry Experiments CalR (version 1.3,
136 https://calrapp.org/(30)). An ANCOVA analysis was performed to determine if there was a significant
137 difference in energy expenditure between the groups.

138 **Assessment of glucose tolerance and insulin tolerance**

139 For GTT, experimental and control mice at 10 weeks post viral inoculation were fasted for 15 hr
140 (6:00 pm – 9:00 am). A sterile glucose solution was intraperitoneally administered at a concentration of 2
141 g/kg (glucose/body weight) at time 0. The blood glucose levels were measured at 15, 30, 60, 90, and 120
142 min after glucose injection. Blood glucose levels vs. time after glucose injection were plotted, and the
143 area under the curve was calculated and compared between the experimental and control groups.

144 For ITT, mice were fasted for 5 hr (9:00 am to 2:00 pm). Blood glucose levels were measured at
145 0, 15, 30, 60, 90, and 120 min following i.p. injection of insulin (1 U/kg). We immediately injected
146 glucose (2 g/kg) if the mice appeared ill due to insulin-induced hypoglycemia.

147 **RT-qPCR analysis**

148 BAT tissues were homogenized in a Trizol reagent (ThermoFisher Scientific, 15596-018), and the
149 total RNA was isolated according to the manufacturer's instructions. First-strand cDNA was synthesized
150 using the SuperScript III First-Strand synthesis kit (ThermoFisher Scientific, 18080-051). qPCR was

151 performed in sealed 96-well plates with SYBR Green I master Mix (Applied Biosystems, A25742) using
152 a Quant Studio 3 (Applied Biosystems). qPCR reactions were prepared in a final volume of 20 µl
153 containing 2 µl cDNAs, and 10 µl of SYBR Green master mix in the presence of primers at 0.5 µM. *beta-*
154 *2 microglobulin (B2m)* was used as an internal control for quantification of each sample. Amplification
155 was performed under the following conditions: denaturation at 95°C for 30 seconds, followed by 40
156 cycles of denaturation at 95°C for 30 seconds, and annealing/extension at 60°C for 1 minute. The primer
157 sequences used are described in Table 1. The relative expression levels were determined using the
158 comparative threshold cycle (CT), which was normalized against the CT of *B2m* using the $^{\Delta\Delta}Ct$ method.

159 **Measurement of plasma leptin, insulin, and L-lactate**

160 Blood samples were collected from the retro-orbital plexus with heparinized capillary tubes
161 (ThermoFisher Scientific, 22-362-566) and then centrifuged at 13,000 rpm for 10 min at 4°C. Plasma
162 leptin and insulin levels were measured using the ELISA kits (ThermoFisher Scientific, KMC2281 for
163 leptin, and Mercodia, 10-1247-01 for insulin, respectively). Plasma L-lactate levels were measured using
164 a colorimetric assay kit (Sigma-Aldrich, MAK065 for L-Lactate).

165 **Immunofluorescence staining**

166 Mice were anesthetized with isoflurane (3%) and transcardially perfused with pre-perfusion
167 solution (9 g NaCl, 5 g sodium nitrate, 10,000 U heparin in 1L distilled water) followed by 4%
168 paraformaldehyde solution. BAT tissues were removed and incubated in 4% paraformaldehyde overnight
169 at 4°C and then placed into 30% sucrose solution for 2-3 days. BAT tissues were sectioned in 20 µm
170 using a Lecia CM3050S cryostat. The sections were blocked in 0.1 M PBS buffer containing 0.2 M
171 glycine (Sigma-Aldrich Cat#G8898, 0.1% triton X-100 (Sigma-Aldrich Cat#X100), 10% normal donkey
172 serum (Sigma-Aldrich Cat#S30) and 1% bovine serum albumin (Sigma-Aldrich Cat#A7906) for 1 hr at
173 room temperature and then incubated with a rabbit anti-HCAR1 antibody (1:200, Alomone, AHR-011)
174 for overnight at the cold room. And then, the sections were washed 3 times in PBS and incubated with
175 Alexa 568 anti-rabbit IgG (1:1000; Life Technologies, Cat#A10042) for 2 hr at room temperature. The
176 sections were washed, dried, and mounted with VECTASHIELD media containing DAPI. Images were
177 acquired using a Leica SP8 confocal microscope.

178 **Western Blotting**

179 Total membrane and cytoplasmic protein fractions were isolated from BAT with a Mem-PER
180 Plus membrane protein extraction kit (Pierce Protein Biology Cat#89842) in the presence of a protease
181 inhibitor/phosphatase inhibitor cocktail (ThermoFisher Scientific Cat#78443). Protein concentrations
182 were determined using a BCA protein assay kit (ThermoFisher scientific Cat#23225). Cytosolic and
183 membrane fraction proteins (30 ug each) were prepared by adding laemmli sample buffer (Bio-Rad,
184 Cat#1610747). Cytosolic proteins were heated at 95°C for 5min and membrane fraction samples were left

185 at room temperature. After sample heating, the samples were separated by 10% SDS-PAGE and
186 transferred to the PVDF membrane. The PVDF membrane was incubated with 5% w/v nonfat dry milk
187 for 1hr at room temperature and immunoblotted with anti-UCP1(1:1000, Abcam Cat#Ab234430), anti-
188 HSL (phospho-serine 660) (1:1000, Cell Signaling Technology Cat#45804S), anti-HSL (1:1000, Cell
189 Signaling Technology Cat#4107), anti-HCAR1 (1:500, Invitrogen Cat#PA5-75664), anti-GAPDH
190 (1:3000, Invitrogen Cat#PA1-987), anti-GLUT4 (1:1,000, Invitrogen Cat#PA1-1065), and anti-Pan-
191 Cadherin (1ug, Cell Signaling Technology Cat#4068T) antibodies. Following incubation in primary
192 antibodies, the membrane was washed three times in TBS-T and then incubated with an anti-rabbit IgG,
193 HRP-linked antibody (1:10,000, Cell signaling Technology Cat#7074) for 2 hr at room temperature. ECL
194 reagents were applied to the membrane and protein bands were detected using an Odyssey Fc imaging
195 system (Li-COR).

196 **Measurement of 2-deoxy-D-glucose (2-DG) uptake**

197 2-DG uptake by BAT was measured with a 2-DG uptake measurement kit (Cosmo bio co., ltd.,
198 CSR-OKP-PMG-K01TE). Mice received an i.p. injection of 2-DG (32.8 ug/kg (31), FisherThermo
199 Scientific, AC111980050) 3 hr post i.p. injection of 3,5-DHBA (200 mg/kg). BAT samples (10 mg) from
200 BAT^{GFP} and BAT^{HCAR1} mice were isolated 1 hr post i.p. injection of 2-DG. And then, the samples were
201 immediately frozen and kept at -80ºC until use. The BAT samples were homogenized with a handheld
202 homogenizer and lysed in 10 mM Tris-HCl (pH8.1) on ice. 2-DG uptake was measured by quantifying 2-
203 DG6P accumulation in BAT following the manufacturer's instructions. The optical density of samples
204 was measured at a wavelength of 420 nm using a microplate reader.

205 **Statistics**

206 All statistical results were presented as mean ± SEM. Statistical analyses were performed using
207 Graphpad Prism 9.0. Two-tailed *t*-tests were used to calculate p values of pair-wise comparisons. Data for
208 comparisons across more than two groups were analyzed using a one-way ANOVA with Tukey's *post*
209 *hoc* comparisons. Time course comparisons between groups were analyzed using a two-way repeated-
210 measures ANOVA with Sidak's correction for multiple comparisons. Data were considered significantly
211 different when the probability value was less than 0.05.

212

213 **Results**

214 **Overexpressing HCAR1 in BAT promotes glucose uptake and nonshivering thermogenesis.**

215 We previously demonstrated *Hcar1* mRNA and protein expression in mouse BAT (27). To
216 extend and further confirm our prior finding, we stained BAT sections with an anti-HCAR1 antibody and
217 found that HCAR1 was detected in the plasma membrane in BAT (Fig. 1A). Hence, RT-qPCR, Western
218 blot, and immunohistochemical analyses support HCAR1 expression in BAT.

219 As *Hcar1* mRNA and protein levels were downregulated in the adipose tissue of male DIO and
220 *ob/ob* mice (27-29), we investigated if HCAR1 overexpression in BAT can restore the capability of BAT
221 in male DIO mice. To overexpress HCAR1 in BAT, we bilaterally injected AAV-HCAR1-GFP
222 (BAT^{HCAR1}) or AAV-GFP (BAT^{GFP}) viruses into the BAT pads of male DIO mice (Fig. 1B). Following
223 viral infection, animals were maintained on HFD for 10 weeks. To validate *Hcar1* overexpression in BAT,
224 we collected BAT at 10 weeks post viral inoculation and performed RT-qPCR. As expected, the *Hcar1*
225 gene expression in BAT was significantly higher in BAT^{HCAR1} mice than in BAT^{GFP} mice (Fig. 1C). The
226 overexpression was further supported by Western blot analysis (Fig. 1C). BAT^{HCAR1} mice exhibited
227 higher levels of HCAR1 expression than the control group. As activation of HCAR1 in BAT caused
228 glucose uptake (27), we examined if the increased HCAR1 expression in BAT improves the ability of
229 BAT to take up circulating glucose in response to treatment with the HCAR1 agonist. Treatment with the
230 HCAR1 agonist 3,5-DHBA significantly increased 2-deoxy-glucose (2-DG) uptake by BAT (Fig. 1D),
231 demonstrating the efficacity and feasibility of our viral vector-mediated overexpression of HCAR1 in
232 BAT.
233 Given that activating HCAR1 signaling promoted glucose uptake (27) and that intracellular
234 glycolysis was involved in heat production in BAT (11, 20), we sought to determine if HCAR1
235 overexpression can cause heat generation in BAT. We directly implanted miniature radio frequency
236 identification (RFID) transponders with an integrated temperature biosensor underneath the BAT pads
237 following viral inoculation and continuously measured BAT temperature. At 3 weeks post viral injection,
238 BAT temperature in BAT^{HCAR1} mice was significantly higher than that in BAT^{GFP} mice during the dark
239 period (Fig. 1E). To examine if this increase is associated with an upregulation of the thermogenic genes
240 in BAT, we evaluated mRNA expression of uncoupling protein 1 (*Ucp1*), peroxisome proliferator-
241 activated receptor-γ coactivator (PGC)-1α (*Pgc1α*), and iodothyronine deiodinase 2 (*Dio2*). UCP1
242 uncouples respiration from ATP synthesis and promotes energy dissipation in the form of heat (32). PGC-
243 1α acts as a transcriptional coactivator that drives UCP1 expression and DIO2 causes a conversion of
244 thyroxin (T4) to 3,3′,5-triiodothyronine (T3), which is a key event in the thermogenic response of BAT to
245 cold-challenge (32). We found that BAT^{HCAR1} mice displayed significant increases in *Ucp1* and *Pgc1α*
246 expression (Fig. 1F), whereas there was no difference in *Dio2* expression between the groups (Fig. 1F). In
247 addition, BAT in BAT^{HCAR1} mice was tan to red in color, whereas BAT^{GFP} mice exhibited the whitening
248 of BAT (Fig. 1G). UCP1 content in BAT was higher in BAT^{HCAR1} mice than in BAT^{GFP} mice (Fig. 1H).
249 Hence, our results support the interpretation that HCAR1 overexpression in BAT improves the ability of
250 BAT to produce heat in male DIO mice under resting conditions.
251 **BAT^{HCAR1} mice are protected from DIO and exhibit improved insulin sensitivity.**

252 Excessive body weight gain in male DIO and *ob/ob* mice was inversely related to HCAR1
253 expression in adipocytes (27-29). We examined if HCAR1 overexpression prevents excessive body
254 weight gain in males during high-fat feeding. As shown in Fig. 2A, BAT^{HCAR1} mice did not gain as much
255 weight as the control group. The difference in body weight between the two groups was observed as early
256 as 3 weeks after viral inoculation and became more profound by the end of the experiments. In line with
257 this finding, BAT^{HCAR1} mice displayed a significant reduction in both fat and lean mass (Fig. 2B and C).
258 These findings support the interpretation that HCAR1 overexpression reduces susceptibility to diet-
259 induced obesity in male mice.
260 We next investigated if there is a difference in energy expenditure between the groups by placing
261 mice in metabolic cages. We found that there was no significant difference in energy expenditure between
262 the groups (total, dark and light phases; Fig. 2D-F). The respiratory exchange ratio (RER) that determines
263 the relative participation of glucose, lipids, and proteins in energy production was significantly different
264 (Fig. 2G). It seems likely that lipids are the predominant fuel source in BAT^{HCAR1} mice. There was no
265 significant difference in locomotor activity between BAT^{GFP} and BAT^{HCAR1} mice (Fig. 2H and I).
266 Prior studies showed increased plasma lactate levels in obese animals and humans (33-38),
267 suggesting that there is a positive correlation between body weight gain and lactate levels. Thus, we
268 evaluated plasma lactate levels in BAT^{HCAR1} and BAT^{GFP} mice. Plasma lactate levels were significantly
269 higher in BAT^{GFP} mice than in BAT^{HCAR1} mice (Fig. 3A), suggesting that the degree of HCAR1
270 expression in BAT rather than lactate levels in circulation may be critical in regulating body weight gain.
271 As BAT^{HCAR1} mice exhibited reduced fat mass compared to controls, we further assessed plasma leptin
272 and insulin levels. BAT^{HCAR1} mice showed significantly lower plasma leptin and insulin levels than the
273 control group (Fig. 3B and C).
274 Given that BAT^{HCAR1} mice exhibited reduced body weight, leptin, and insulin levels, we further
275 examined if BAT^{HCAR1} mice display improved glucose and insulin tolerance. First, we measured basal
276 (non-fasting) and fasting glucose levels. BAT^{HCAR1} mice showed lower basal blood glucose levels than
277 the control group, although there was no significant difference in fasting glucose levels (Fig. 3D and E).
278 We then performed glucose tolerance tests to assess the ability of BAT^{HCAR1} mice to dispose of
279 a glucose load. We found a significant improvement in glucose tolerance in BAT^{HCAR1} mice compared to
280 controls (Fig. 3F). We also carried out insulin tolerance tests to assess glucose levels over time to an i.p.
281 insulin injection. BAT^{HCAR1} mice displayed a robust increase in insulin sensitivity (Fig. 3G). These
282 findings suggest that HCAR1 in BAT may contribute to the regulation of glucose homeostasis in DIO
283 mice.
284 Next, we sought to determine if the effects of HCAR1 are coupled to changes in nutrient
285 availability, we overexpressed HCAR1 in BAT in mice fed LFD (Fig. 4A). Unlike DIO mice, there was

286 no significant difference in body weight between the control (mice^{GFP}) and experimental groups
287 (mice^{HCAR1}) (Fig. 4B). In addition, the percentages of fat and lean mass were similar between the two
288 groups (Fig. 4C and D). We also looked at if overexpressing HCAR1 in BAT changes glucose tolerance
289 and insulin sensitivity in mice fed LFD. We found that mice overexpressing HCAR1 in BAT exhibited
290 similar basal and fasting blood glucose levels (Fig. 4E and F) and no improvement in glucose and insulin
291 tolerance (Fig. 4G and H). Moreover, overexpressing HCAR1 did not alter plasma leptin and insulin
292 levels (Fig. 4I and J). These results suggest that the metabolic effects of HCAR1 appear to be coupled
293 with changes in nutrient availability.
294 **HCAR1 overexpression upregulates GLUT4 expression and reduces HSL phosphorylation.**
295 As improved glucose disposal would be due in part to increased glucose transporter expression
296 and translocation in BAT, we evaluated mRNA expression levels of the glucose transporter 1 and 4
297 (*Slc2a1 (Glut1)* and *Slc2a4 (Glut4)*) in BAT of BAT^{HCAR1} and BAT^{GFP} mice on high-fat feeding. We
298 found that HCAR1 overexpression markedly increased *Slc2a4* mRNA expression in BAT (Fig. 5A).
299 Western blot analysis further revealed higher levels of cytosolic GLUT4 expression in BAT^{HCAR1} mice
300 than in BAT^{GFP} mice (Fig. 5B), consistent with increased *Slc2a4* gene expression. Insulin increased
301 glucose uptake by controlling the trafficking of GLUT4 to the plasma membrane in BAT (39, 40). We
302 further sought to determine if HCAR1 overexpression can also cause GLUT4 translocation to the plasma
303 membrane. Following isolation of the membrane proteins from BAT, we performed Western blotting and
304 found an increase in the plasma membrane GLUT4 expression in BAT^{HCAR1} mice (Fig. 5B). Hence, our
305 results suggest that increased GLUT4 translocation to the plasma membrane may improve glucose
306 tolerance in BAT^{HCAR1} mice.
307 Activation of HCAR1 inhibited lipolysis in white adipocytes *in vitro* and *in vivo* (23, 25). We
308 thus asked if HCAR1 overexpression alters lipid metabolism in BAT of DIO mice by evaluating lipogenic
309 gene expression and hormone-sensitive lipase (HSL) phosphorylation that stimulates triglyceride
310 hydrolysis. Immunoblotting analysis revealed that BAT^{HCAR1} mice exhibited no or little HSL
311 phosphorylation at serine 660, while HSL phosphorylation was detected in BAT of BAT^{GFP} mice (Fig.
312 5C). In addition, RT-qPCR analysis of lipogenic enzyme genes, such as ATP citrate lyase (ACL), acetyl-
313 CoA carboxylase (ACC1), fatty acid synthase (FASN), and stearoyl-CoA desaturase 1 (SCD1) further
314 revealed that BAT^{HCAR1} mice had increased lipogenic enzyme gene expression (Fig. 5D). Hence, our
315 results suggest that HCAR1 overexpression may reduce basal lipolysis, while promoting fatty acid
316 synthesis in BAT during conditions of nutrient excess.
317
318
319

320 **Discussion**

321 The present study demonstrates that HCAR1 in BAT plays a key role in controlling body weight,
322 glucose homeostasis, and insulin sensitivity in male DIO mice. A series of experiments support our
323 conclusion. First, we found that BAT^{HCAR1} mice exhibited increased BAT temperature. Second, BAT^{HCAR1}
324 mice significantly gained less body weight compared to BAT^{GFP} mice. Interestingly, plasma lactate levels
325 in BAT^{HCAR1} mice were lower compared to those in BAT^{GFP} mice. Third, BAT^{HCAR1} mice displayed
326 improved glucose tolerance and insulin sensitivity. Forth, HCAR1 overexpression upregulated the *Slc2a4*
327 gene and caused GLUT4 translocation to the plasma membrane. Finally, this overexpression increased
328 lipogenic gene expression, while reducing HSL phosphorylation. Taken together, our results provide
329 novel insights into the role of lactate and its cognate receptors in BAT in the control of glucose
330 homeostasis in DIO mice.

331 Obese humans and animals had high plasma lactate levels (33-38). In our preparations, obese
332 BAT^{GFP} mice also exhibited higher plasma lactate levels than BAT^{HCAT1} mice, suggesting that there was a
333 positive correlation between body weight and circulating lactate levels. In contrast to increased lactate
334 levels, HCAR1 expression in the adipose tissue was inversely correlated with body mass in male mice
335 (27-29), suggesting that the degree of HCAR1 expression in BAT rather than plasma lactate levels would
336 be a key factor in maintaining metabolic balance in mice. Of particular interest is that treatment with the
337 HCAR1 agonist reduced systemic glucose levels in male DIO mice via increased glucose uptake by BAT
338 (27). Thus, it appears that HCAR1 in BAT remains functional in DIO male mice. It is conceivable that
339 HCAR1 would be an alternative target to control euglycemia in DIO mice as DIO reduced insulin
340 signaling with decreased Akt phosphorylation in BAT, resulting in insulin resistance (41).

341 Pharmacological activation of the sympathetic β3AR in BAT drove glucose uptake and converted
342 glucose to lactate via increased glycolysis (11, 18, 20). Upon lactate production in BAT, lactate was
343 secreted and acted in an autocrine and paracrine manner in rodents and humans (7, 18). In our prior study,
344 optogenetic stimulation of sympathetic nerves innervating BAT upregulated the expression of the *Ldha/b*
345 and *Mct1* genes in BAT (11). Blockade of lactate production and transport by inhibiting LDH and MCT1
346 abolished β3AR-mediated glucose uptake in BAT (11), suggesting the important role of lactate in
347 controlling the ability of BAT to take up circulating glucose. In addition, transgenic mice with increased
348 glucose uptake in WAT by expressing glucokinase displayed increased lactate production (42). They
349 exhibited improved glucose tolerance and insulin sensitivity when fed a standard chow diet (42).
350 Although these transgenic mice became obese similarly to controls when fed HFD, they remained insulin
351 sensitivity (42). Although the Bosch research group did not examine if improved insulin sensitivity was in
352 part due to elevated lactate production in WAT, it is possible that a rise in lactate production may improve
353 glucose tolerance and insulin sensitivity. In fact, increased lactate release from WAT improved the

354 antilipolytic effect of insulin via activation of HCAR1 (23). In line with the previous findings in WAT,
355 BAT^{HCAR1} mice exhibited a reduction in HSL phosphorylation in BAT, resulting in a decrease in basal
356 lipolysis. This antilipolytic effect of HCAR1 in WAT and BAT would be important because basal
357 lipolysis was elevated during obesity and was closely associated with insulin resistance (43). Reduced
358 basal lipolysis in the adipose tissue would lead to improved insulin sensitivity. Hence, it is conceivable
359 that not only lactate production but also its cognate receptor in the adipose tissue is indispensable for
360 maintaining euglycemia and insulin sensitivity in lean and obese animals.
361 The Offermanns' research group demonstrated that adipocytes used HCAR1-mediated lactate
362 signaling as an indirect index of glucose availability (23). Namely, activation of HCAR1 by lactate
363 released from adipocytes inhibited lipolysis, resulting in an increase in energy storage in the form of
364 triglycerides when blood glucose levels were high (23). Despite the antilipolytic effect of HCAR1,
365 HCAR1 KO mice exhibited no significant differences in body weight, glucose tolerance and insulin
366 sensitivity in mice fed a standard chow diet and HFD (23). When HCAR1 was overexpressed in BAT of
367 mice fed LFD, we also found no changes in body weight and glucose homeostasis, consistent with the
368 study by the Offermanns' group. Unlike the HCAR1 KO mice on HFD, however, BAT^{HCAR1} mice
369 significantly gained less body weight than BAT^{GFP} mice kept on HFD, suggesting that increased BAT
370 activity in BAT^{HCAR1} mice could prevent body weight gain. In fact, the ability of BAT to control body
371 weight has been well described in mice receiving BAT transplant (44-46). Importantly, increased BAT
372 activity in mice receiving BAT transplant led to a reduction in body weight in *ob*/*ob* mice (46). The
373 improvement of energy metabolism in mice receiving BAT transplant appears to be mediated by
374 adipokines released from BAT, including fibroblast growth factor 21, interleukin 6, and tumor necrosis
375 factor-a (44, 47). However, it was also suggested that BAT secretes other adipokines that work through
376 insulin-independent pathways (46). Hence, our current study suggests that lactate is an understudied
377 signal molecule released from BAT. The interaction between lactate and HCAR1 in BAT can enhance
378 BAT activity that improves whole-body energy metabolism and insulin sensitivity, particularly in obese
379 animals.
380 What are the cellular mechanisms underlying the anti-obesity effect of HCAR1 in BAT? We have
381 no clear explanation for this anti-obesity effect. In fact, we failed to detect a significant difference in
382 energy expenditure between the groups at the end of 10 weeks of high-fat feeding. However, we may not
383 exclude the possibility that an accumulation of small improvements in basal metabolic rate after starting
384 high-fat feeding in BAT^{HCAR1} mice may prevent body weight gain during high-fay feeding. In addition, it
385 has been shown that, unlike WAT, BAT is metabolically active under resting conditions in humans (7). In
386 other words, BAT actively took up circulating glucose and released lactate regardless of heat production
387 (7). In our preparations, increased HCAR1 expression in BAT promoted *Slc2A4* mRNA and protein

388 expression. More importantly, BAT^{HCAR1} mice showed increased GLUT4 trafficking to the plasma
389 membrane. GLUT4 trafficking in BAT was a prerequisite for augmented glucose uptake by BAT in
390 rodents and humans (8, 10, 48). Thus, BAT in BAT^{HCAR1} mice can substantially take up glucose under
391 resting conditions. In fact, basal non-fasting glucose levels in BAT^{HCAR1} mice were significantly lower
392 compared to those in BAT^{GFP} mice. Lactate produced by increased glucose entry would be transported out
393 of the cell and concomitant activation of HCAR1 would inhibit lipolysis and trigger fatty acid synthesis,
394 resulting in increased energy storage as described in human BAT (7). This possibility was supported by
395 our findings showing a robust upregulation of lipogenic gene expression in BAT of BAT^{HCAR1} mice and
396 inhibition of lipolysis in BAT.
397 Additionally, lactate is a major substrate for the TCA cycle in all tissues, including adipose tissue
398 (49). We previously showed that blockade of the MCT1 completely abolished the thermogenic effect of
399 the activation of β3AR (11). Hence, it is plausible that lactate might be transported to mitochondria, feed
400 the TCA cycle, and generate heat in BAT. As obese mice have diminished thermogenic capacity
401 compared to lean mice (50), increased BAT activity in BAT^{HCAR1} mice would contribute to body weight
402 loss under a hypercaloric diet. Taken together, our current study showed that, like insulin receptors,
403 HCAR1 expressed in BAT could promote glucose entry and reduce lipolysis, resulting in body weight
404 loss and insulin sensitivity. Hence, targeting HCAR1 in BAT would provide an alternative way to control
405 body weight and euglycemia in individuals with obesity.
406
407
408
409

410 **Acknowledgments**

411 **General**: We thank Drs. Gary Schwartz and Streamson Chua Jr. for their valuable feedback and
412 comments on this study. We also thank Dr. Shun-Mei Liu and Licheng Wu for their technical assistance.

413 **Funding:** This work was supported by the NIH (RO1 DK092246, R01 AT011653, R03 TR003313, and
414 P30 DK020541) to Y.-H.J.

415 **Author contributions:** HY carried out viral injection, metabolic phenotyping, real-time qRT-PCR,
416 ELISA assays, and analyzed data. JY carried out viral injection, immunostaining, Western
417 blotting, ELISA assays, and analyzed data. Y.-H. designed research, performed viral injection
418 immunocytochemistry, analyzed the data, and wrote the manuscript.
419

420 **Competing interests:** There are no competing interests.
421

422 **References**

423 1. **Cypess AM, Weiner LS, Roberts-Toler C, Franquet Elia E, Kessler SH, Kahn PA,**
424 **English J, Chatman K, Trauger SA, Doria A, and Kolodny GM**. Activation of human brown
425 adipose tissue by a beta3-adrenergic receptor agonist. *Cell Metab* 21: 33-38, 2015.
426 2. **Saito M, Okamatsu-Ogura Y, Matsushita M, Watanabe K, Yoneshiro T, Nio-**
427 **Kobayashi J, Iwanaga T, Miyagawa M, Kameya T, Nakada K, Kawai Y, and Tsujisaki M**.
428 High incidence of metabolically active brown adipose tissue in healthy adult humans: effects of
429 cold exposure and adiposity. *Diabetes* 58: 1526-1531, 2009.
430 3. **Ouellet V, Labbe SM, Blondin DP, Phoenix S, Guerin B, Haman F, Turcotte EE,**
431 **Richard D, and Carpentier AC**. Brown adipose tissue oxidative metabolism contributes to
432 energy expenditure during acute cold exposure in humans. *J Clin Invest* 122: 545-552, 2012.
433 4. **Matsushita M, Yoneshiro T, Aita S, Kameya T, Sugie H, and Saito M**. Impact of
434 brown adipose tissue on body fatness and glucose metabolism in healthy humans. *Int J Obes*
435 *(Lond)* 38: 812-817, 2014.
436 5. **Chondronikola M, Volpi E, Borsheim E, Porter C, Annamalai P, Enerback S, Lidell**
437 **ME, Saraf MK, Labbe SM, Hurren NM, Yfanti C, Chao T, Andersen CR, Cesani F,**
438 **Hawkins H, and Sidossis LS**. Brown adipose tissue improves whole-body glucose homeostasis
439 and insulin sensitivity in humans. *Diabetes* 63: 4089-4099, 2014.
440 6. **Lee P, Smith S, Linderman J, Courville AB, Brychta RJ, Dieckmann W, Werner**
441 **CD, Chen KY, and Celi FS**. Temperature-acclimated brown adipose tissue modulates insulin
442 sensitivity in humans. *Diabetes* 63: 3686-3698, 2014.
443 7. **Weir G, Ramage LE, Akyol M, Rhodes JK, Kyle CJ, Fletcher AM, Craven TH,**
444 **Wakelin SJ, Drake AJ, Gregoriades ML, Ashton C, Weir N, van Beek EJR, Karpe F,**
445 **Walker BR, and Stimson RH**. Substantial Metabolic Activity of Human Brown Adipose Tissue
446 during Warm Conditions and Cold-Induced Lipolysis of Local Triglycerides. *Cell Metab* 27:
447 1348-1355 e1344, 2018.
448 8. **Lee P, Bova R, Schofield L, Bryant W, Dieckmann W, Slattery A, Govendir MA,**
449 **Emmett L, and Greenfield JR**. Brown Adipose Tissue Exhibits a Glucose-Responsive
450 Thermogenic Biorhythm in Humans. *Cell Metab* 23: 602-609, 2016.
451 9. **M UD, Saari T, Raiko J, Kudomi N, Maurer SF, Lahesmaa M, Fromme T, Amri EZ,**
452 **Klingenspor M, Solin O, Nuutila P, and Virtanen KA**. Postprandial Oxidative Metabolism of
453 Human Brown Fat Indicates Thermogenesis. *Cell Metab* 28: 207-216 e203, 2018.
454 10. **Orava J, Nuutila P, Lidell ME, Oikonen V, Noponen T, Viljanen T, Scheinin M,**
455 **Taittonen M, Niemi T, Enerback S, and Virtanen KA**. Different metabolic responses of
456 human brown adipose tissue to activation by cold and insulin. *Cell Metab* 14: 272-279, 2011.
457 11. **Jeong JH, Chang JS, and Jo YH**. Intracellular glycolysis in brown adipose tissue is
458 essential for optogenetically induced nonshivering thermogenesis in mice. *Sci Rep* 8: 6672, 2018.
459 12. **Hankir MK, Cowley MA, and Fenske WK**. A BAT-Centric Approach to the Treatment
460 of Diabetes: Turn on the Brain. *Cell Metab* 2016.
461 13. **Townsend KL, and Tseng YH**. Brown fat fuel utilization and thermogenesis. *Trends*
462 *Endocrinol Metab* 25: 168-177, 2014.
463 14. **Hankir MK, Kranz M, Keipert S, Weiner J, Andreasen SG, Kern M, Patt M,**
464 **Kloting N, Heiker JT, Brust P, Hesse S, Jastroch M, and Fenske WK**. Dissociation Between
465 Brown Adipose Tissue (18)F-FDG Uptake and Thermogenesis in Uncoupling Protein 1-
466 Deficient Mice. *J Nucl Med* 58: 1100-1103, 2017.

15. **Shin H, Ma Y, Chanturiya T, Cao Q, Wang Y, Kadegowda AKG, Jackson R, Rumore D, Xue B, Shi H, Gavrilova O, and Yu L**. Lipolysis in Brown Adipocytes Is Not Essential for Cold-Induced Thermogenesis in Mice. *Cell Metab* 2017.

16. **Olsen JM, Csikasz RI, Dehvari N, Lu L, Sandstrom A, Oberg AI, Nedergaard J, Stone-Elander S, and Bengtsson T**. beta3-Adrenergically induced glucose uptake in brown adipose tissue is independent of UCP1 presence or activity: Mediation through the mTOR pathway. *Mol Metab* 6: 611-619, 2017.

17. **Shackney SE, and Joel CD**. Stimulation of glucose metabolism in brown adipose tissue by addition of insulin in vitro. *J Biol Chem* 241: 4004-4010, 1966.

18. **Ma SW, and Foster DO**. Uptake of glucose and release of fatty acids and glycerol by rat brown adipose tissue in vivo. *Can J Physiol Pharmacol* 64: 609-614, 1986.

19. **Hao Q, Yadav R, Basse AL, Petersen S, Sonne SB, Rasmussen S, Zhu Q, Lu Z, Wang J, Audouze K, Gupta R, Madsen L, Kristiansen K, and Hansen JB**. Transcriptome profiling of brown adipose tissue during cold exposure reveals extensive regulation of glucose metabolism. *Am J Physiol Endocrinol Metab* 308: E380-392, 2015.

20. **Winther S, Isidor MS, Basse AL, Skjoldborg N, Cheung A, Quistorff B, and Hansen JB**. Restricting glycolysis impairs brown adipocyte glucose and oxygen consumption. *Am J Physiol Endocrinol Metab* 314: E214-E223, 2018.

21. **Iwanaga T, Kuchiiwa T, and Saito M**. Histochemical demonstration of monocarboxylate transporters in mouse brown adipose tissue. *Biomed Res* 30: 217-225, 2009.

22. **Lagarde D, Jeanson Y, Barreau C, Moro C, Peyriga L, Cahoreau E, Guissard C, Arnaud E, Galinier A, Bouzier-Sore AK, Pellerin L, Chouchani ET, Penicaud L, Ader I, Portais JC, Casteilla L, and Carriere A**. Lactate fluxes mediated by the monocarboxylate transporter-1 are key determinants of the metabolic activity of beige adipocytes. *J Biol Chem* 296: 100137, 2021.

23. **Ahmed K, Tunaru S, Tang C, Muller M, Gille A, Sassmann A, Hanson J, and Offermanns S**. An autocrine lactate loop mediates insulin-dependent inhibition of lipolysis through GPR81. *Cell Metab* 11: 311-319, 2010.

24. **Wang GX, Zhao XY, and Lin JD**. The brown fat secretome: metabolic functions beyond thermogenesis. *Trends Endocrinol Metab* 26: 231-237, 2015.

25. **Liu C, Wu J, Zhu J, Kuei C, Yu J, Shelton J, Sutton SW, Li X, Yun SJ, Mirzadegan T, Mazur C, Kamme F, and Lovenberg TW**. Lactate inhibits lipolysis in fat cells through activation of an orphan G-protein-coupled receptor, GPR81. *J Biol Chem* 284: 2811-2822, 2009.

26. **Ge H, Weiszmann J, Reagan JD, Gupte J, Baribault H, Gyuris T, Chen JL, Tian H, and Li Y**. Elucidation of signaling and functional activities of an orphan GPCR, GPR81. *J Lipid Res* 49: 797-803, 2008.

27. **Kwon E, Yoo T, Joung HY, and Jo YH**. Hydrocarboxylic acid receptor 1 in BAT regulates glucose uptake in mice fed a high-fat diet. *PLoS One* 15: e0228320, 2020.

28. **Wanders D, Graff EC, and Judd RL**. Effects of high fat diet on GPR109A and GPR81 gene expression. *Biochem Biophys Res Commun* 425: 278-283, 2012.

29. **Feingold KR, Moser A, Shigenaga JK, and Grunfeld C**. Inflammation inhibits GPR81 expression in adipose tissue. *Inflamm Res* 60: 991-995, 2011.

30. **Mina AI, LeClair RA, LeClair KB, Cohen DE, Lantier L, and Banks AS**. CalR: A Web-Based Analysis Tool for Indirect Calorimetry Experiments. *Cell Metab* 28: 656-666 e651, 2018.

31. **Albert V, Svensson K, Shimobayashi M, Colombi M, Munoz S, Jimenez V, Handschin C, Bosch F, and Hall MN**. mTORC2 sustains thermogenesis via Akt-induced glucose uptake and glycolysis in brown adipose tissue. *EMBO Mol Med* 8: 232-246, 2016.
32. **Tabuchi C, and Sul HS**. Signaling Pathways Regulating Thermogenesis. *Front Endocrinol (Lausanne)* 12: 595020, 2021.
33. **Arriaran S, Agnelli S, Sabater D, Remesar X, Fernandez-Lopez JA, and Alemany M**. Evidences of basal lactate production in the main white adipose tissue sites of rats. Effects of sex and a cafeteria diet. *PLoS One* 10: e0119572, 2015.
34. **Chen CJ, Liao YH, Lin SY, Yu JX, Li ZJ, Lin YC, Chang GJ, Lin CH, and Wong AM**. Diet-induced obesity accelerates blood lactate accumulation of rats in response to incremental exercise to maximum. *Am J Physiol Regul Integr Comp Physiol* 313: R601-R607, 2017.
35. **Chen YD, Varasteh BB, and Reaven GM**. Plasma lactate concentration in obesity and type 2 diabetes. *Diabete Metab* 19: 348-354, 1993.
36. **Crawford SO, Hoogeveen RC, Brancati FL, Astor BC, Ballantyne CM, Schmidt MI, and Young JH**. Association of blood lactate with type 2 diabetes: the Atherosclerosis Risk in Communities Carotid MRI Study. *Int J Epidemiol* 39: 1647-1655, 2010.
37. **Jansson PA, Larsson A, Smith U, and Lonnroth P**. Lactate release from the subcutaneous tissue in lean and obese men. *J Clin Invest* 93: 240-246, 1994.
38. **Jones TE, Pories WJ, Houmard JA, Tanner CJ, Zheng D, Zou K, Coen PM, Goodpaster BH, Kraus WE, and Dohm GL**. Plasma lactate as a marker of metabolic health: Implications of elevated lactate for impairment of aerobic metabolism in the metabolic syndrome. *Surgery* 166: 861-866, 2019.
39. **Leto D, and Saltiel AR**. Regulation of glucose transport by insulin: traffic control of GLUT4. *Nat Rev Mol Cell Biol* 13: 383-396, 2012.
40. **Skorobogatko Y, Dragan M, Cordon C, Reilly SM, Hung CW, Xia W, Zhao P, Wallace M, Lackey DE, Chen XW, Osborn O, Bogner-Strauss JG, Theodorescu D, Metallo CM, Olefsky JM, and Saltiel AR**. RalA controls glucose homeostasis by regulating glucose uptake in brown fat. *Proc Natl Acad Sci U S A* 115: 7819-7824, 2018.
41. **Roberts-Toler C, O'Neill BT, and Cypess AM**. Diet-induced obesity causes insulin resistance in mouse brown adipose tissue. *Obesity (Silver Spring)* 23: 1765-1770, 2015.
42. **Munoz S, Franckhauser S, Elias I, Ferre T, Hidalgo A, Monteys AM, Molas M, Cerdan S, Pujol A, Ruberte J, and Bosch F**. Chronically increased glucose uptake by adipose tissue leads to lactate production and improved insulin sensitivity rather than obesity in the mouse. *Diabetologia* 53: 2417-2430, 2010.
43. **Morigny P, Houssier M, Mouisel E, and Langin D**. Adipocyte lipolysis and insulin resistance. *Biochimie* 125: 259-266, 2016.
44. **Stanford KI, Middelbeek RJ, Townsend KL, An D, Nygaard EB, Hitchcox KM, Markan KR, Nakano K, Hirshman MF, Tseng YH, and Goodyear LJ**. Brown adipose tissue regulates glucose homeostasis and insulin sensitivity. *J Clin Invest* 123: 215-223, 2013.
45. **Liu X, Zheng Z, Zhu X, Meng M, Li L, Shen Y, Chi Q, Wang D, Zhang Z, Li C, Li Y, Xue Y, Speakman JR, and Jin W**. Brown adipose tissue transplantation improves whole-body energy metabolism. *Cell Res* 23: 851-854, 2013.
46. **Liu X, Wang S, You Y, Meng M, Zheng Z, Dong M, Lin J, Zhao Q, Zhang C, Yuan X, Hu T, Liu L, Huang Y, Zhang L, Wang D, Zhan J, Jong Lee H, Speakman JR, and Jin**

557 **W**. Brown Adipose Tissue Transplantation Reverses Obesity in Ob/Ob Mice. *Endocrinology* 156:
558 2461-2469, 2015.
559 47. **Gunawardana SC, and Piston DW**. Reversal of type 1 diabetes in mice by brown
560 adipose tissue transplant. *Diabetes* 61: 674-682, 2012.
561 48. **Picatoste B, Yammine L, Leahey RA, Soares D, Johnson EF, Cohen P, and McGraw**
562 **TE**. Defective insulin-stimulated GLUT4 translocation in brown adipocytes induces systemic
563 glucose homeostasis dysregulation independent of thermogenesis in female mice. *Mol Metab* 53:
564 101305, 2021.
565 49. **Hui S, Ghergurovich JM, Morscher RJ, Jang C, Teng X, Lu W, Esparza LA, Reya**
566 **T, Le Z, Yanxiang Guo J, White E, and Rabinowitz JD**. Glucose feeds the TCA cycle via
567 circulating lactate. *Nature* 2017.
568 50. **Branca RT, He T, Zhang L, Floyd CS, Freeman M, White C, and Burant A**.
569 Detection of brown adipose tissue and thermogenic activity in mice by hyperpolarized xenon
570 MRI. *Proc Natl Acad Sci U S A* 111: 18001-18006, 2014.

571

572 **Figure legends.**

573 **Figure 1. BAT^{HCAR1} mice exhibit increased glucose uptake and BAT temperature.**

574 **A**. Images of confocal fluorescence microscopy showing expression of HCAR1 in BAT (arrowheads).
575 Scale bar: 30μm. Bottom panel: higher magnification view of the area of the white square.

576 **B**. Schematic illustration of our experimental configurations. AAV5-*Hcar1*-GFP (closed circle) and
577 AAV5-GFP (open circle) viruses were bilaterally injected to the BAT pads of male DIO mice. Mice were
578 maintained on high-fat feeding.

579 **C**. Summary plot showing increased expression in *Hcar1* mRNA expression in BAT of BAT^{HCAR1} mice
580 (BAT^{GFP} mice, n= 12 mice, BAT^{HCAR1} mice, n= 9 mice, two-tailed *t*-test, ***p<0.001). Bottom panel:
581 Western blot images showing HCAR1 expression in BAT of BAT^{HCAR1} and BAT^{GFP} mice.

582 **D**. Summary plot showing 2-DG uptake by BAT in response to treatment with the HCAR1 agonist 3,5-
583 DHBA (BAT^{GFP} mice, n= 6 mice, BAT^{HCAR1} mice, n= 4, two-tailed *t*-test, **p<0.01)

584 **E**. Summary plot showing increased BAT temperature in the dark phase in BAT^{HCAR1} (n= 5 mice) and
585 BAT^{GFP} (n= 5 mice) mice. Two-tailed *t*-test, ***p<0.001

586 **F**. Summary plot showing gene expression of the thermogenic genes *Ucp1*, *Pgc1a*, and *Dio2* (BAT^{GFP}
587 mice, n= 7 mice, BAT^{HCAR1} mice, n= 7, two-tailed *t*-test, *p<0.05, **p<0.01)

588 **G**. Images showing BAT morphology in BAT^{GFP} and BAT^{HCAR1} mice.

589 **H**. Western blot images showing UCP1 expression in BAT of BAT^{HCAR1} and BAT^{GFP} mice.

590

591 **Figure 2. BAT^{HCAR1} mice gain less body weight**

592 **A**. Summary plot of body weight obtained from BAT^{GFP} (open circle; n = 11 mice) and BAT^{HCAR1} (closed
593 circle; n = 10 mice, two-way ANOVA test, ***p<0.001). BAT^{HCAR1} mice significantly weighed less than
594 BAT^{GFP} mice.

595 **B** and **C**. Summary plots showing fat and lean mass in BAT^{GFP} (n=14 mice) and BAT^{HCAR1} (n=10 mice)
596 mice (fat mass, two-tailed *t*-test, ***p<0.001; lean mass, **p<0.01).

597 **D, E, and F**. Summary plots showing energy expenditure in BAT^{GFP} (n =5 mice) and BAT^{HCAR1} (n=7
598 mice) mice.

599 **G**. Graph showing RER in BAT^{GFP} and BAT^{HCAR1} mice (*p<0.05).

600 **H and I.** Graphs showing locomotor activity in BAT^{GFP} and BAT^{HCAR1} mice.

601

602 **Figure 3. BAT^{HCAR1} mice display improved glucose and insulin tolerance.**

603 **A**, **B**, and **C**. Summary plots showing plasma lactate, leptin, and insulin levels in BAT^{GFP} and BAT^{HCAR1}
604 mice (lactate, n= 7 vs. 10 mice, two-tailed *t*-test, *p<0.05; leptin, n= 8 vs. 9 mice, two-tailed *t*-test,
605 ***p<0.001; insulin, n= 8 vs. 9 mice, two-tailed *t*-test, ***p<0.001).

606 **D** and **E**. Summary plots showing basal and fasting glucose levels in BAT^{GFP} and BAT^{HCAR1} mice (basal
607 [glucose], n= 10 vs. 9 mice, two-tailed *t*-test, *p<0.05; fasting [glucose], n= 10 vs. 8 mice).
608 **F**. Summary plots showing changes in blood glucose levels in response to i.p. injection of glucose (2g/kg).
609 BAT^{HCAR1} mice showed improved glucose tolerance (BAT^{GFP} mice, n= 7, BAT^{HCAR1} mice, n= 8, two-way
610 ANOVA test, *p<0.05). Right panel: glucose AUC in BAT^{GFP} and BAT^{HCAR1} mice (two tailed *t*-test,
611 *p<0.05)
612 **G**. Summary plot showing changes in blood glucose levels in response to i.p. injection of insulin (1U/kg).
613 Increased insulin sensitivity was observed in BAT^{HCAR1} mice (BAT^{GFP} mice, n= 6, BAT^{HCAR1} mice, n= 8,
614 two-way ANOVA test, ***p<0.001).
615
616 **Figure 4. Overexpressing HCAR1 in BAT doesn't change body weight and glucose homeostasis in**
617 **mice fed LFD.**
618 **A.** Schematic illustration of our experimental configurations. AAV5-*Hcar1*-GFP ($mice^{HCAR1}$, closed circle)
619 and AAV5-GFP ($mice^{GFP}$, open circle) viruses were bilaterally injected to the BAT pads of male mice fed
620 LFD for 10 weeks. Right panel: Pooled data showed increased expression in *Hcar1* mRNA expression in
621 BAT of $mice^{HCAR1}$ ($mice^{GFP}$, n= 6 mice, $mice^{HCAR1}$, n= 13 mice, two-tailed *t*-test, **p<0.01).
622 **B**. Summary plot showing body weight obtained from $mice^{GFP}$ (open circle; n = 12) and $mice^{HCAR1}$ (closed
623 circle; n = 13 mice).
624 **C** and **D**. Summary plots showing percentages of fat and lean mass in $mice^{GFP}$ (n=12) and $mice^{HCAR1}$
625 (n=13) mice.
626 **E** and **F**. Summary plots showing basal and fasting glucose levels in $mice^{GFP}$ and $mice^{HCAR1}$ mice (basal
627 [glucose], n= 8 vs. 6 mice; fasting [glucose], n= 13 vs. 10 mice).
628 **G**. Summary plots showing changes in blood glucose levels in response to i.p. injection of glucose (2g/kg;
629 $mice^{GFP}$, n= 13 mice, $mice^{HCAR1}$, n= 10).
630 **H**. Summary plot showing changes in blood glucose levels in response to i.p. injection of insulin (1U/kg;
631 $mice^{GFP}$ mice, n= 4, $mice^{HCAR1}$ mice, n= 9).
632 **I** and **J**. Summary plots showing plasma leptin and insulin levels in $mice^{GFP}$ and $mice^{HCAR1}$ mice (leptin,
633 n= 8 vs. 10 mice; insulin, n= 9 vs. 9 mice). No significant differences were found in all the parameters (B-
634 J, two-tailed t-test and two-way ANOVA test).
635
636 **Figure 5. HCAR1 overexpression in BAT reduces HSL phosphorylation, while upregulating mRNA**
637 **expression of the lipogenic genes in DIO mice**.
638 **A**. Summary plot showing mRNA expression of *Slc2a1* and *Slc2a4* in BAT of BAT^{GFP} and BAT^{HCAR1}
639 mice. Both *Slc2a1* and *Slc2a4* expression was significantly upregulated by HCAR1 overexpression in

640 BAT (*Slc2a1*, BAT^{GFP} mice, n= 7 mice; BAT^{HCAR1} mice, n= 7 mice, two-tailed *t*-test, *p<0.05; *Slc2a4,*
641 BAT^{GFP} mice, n= 7 mice; BAT^{HCAR1} mice, n= 7 mice, two-tailed *t*-test, ***p<0.001).
642 **B**. Western blot images showing cytosolic and membrane GLUT4 expression in BAT
643 **C**. Western blot images showing reduced HSL phosphorylation at serine 660 in BAT of BAT^{HCAR1} mice.
644 **D**. Summary plots showing upregulated mRNA expression of the lipogenic enzyme genes in BAT of
645 BAT^{HCAR1} mice (BAT^{GFP} mice, n= 7 mice; BAT^{HCAR1} mice, n= 7 mice, two-tailed *t*-test, **p<0.01,
646 ***p<0.001). Left panel: schematic diagram describing lipogenic enzymes involved in the synthesis of
647 fatty acids in BAT.
648
649

Figure 1

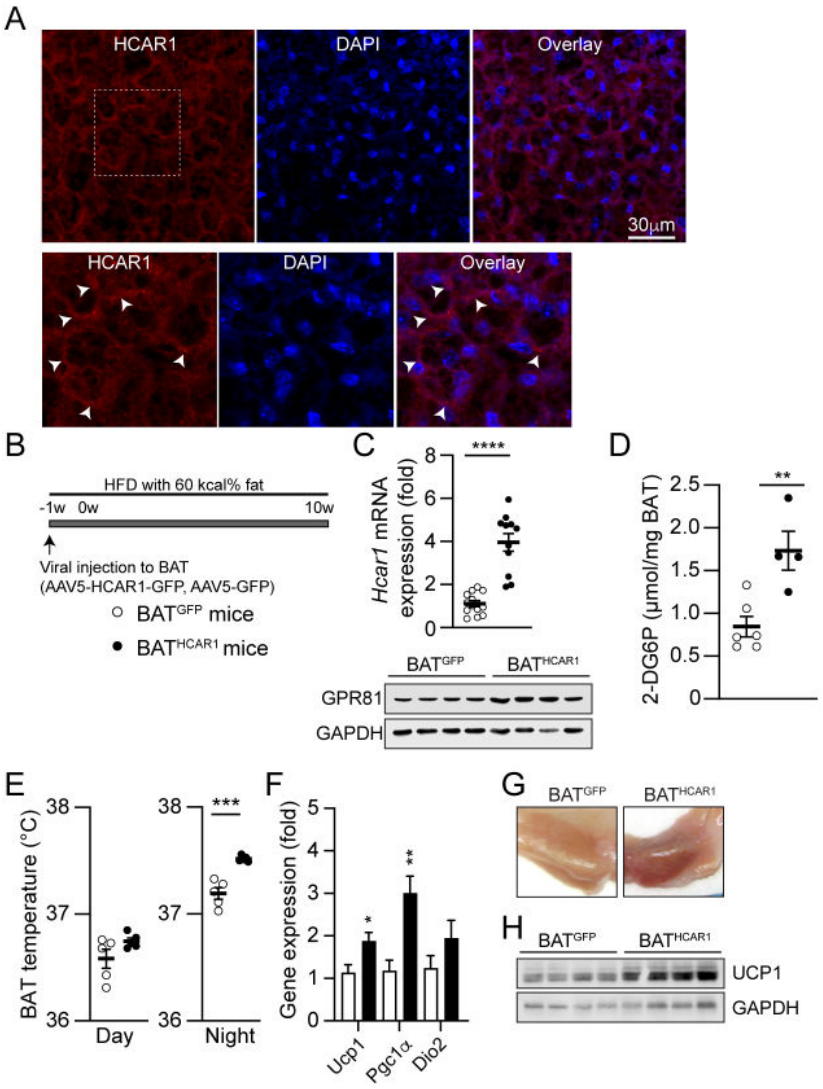

Figure 2

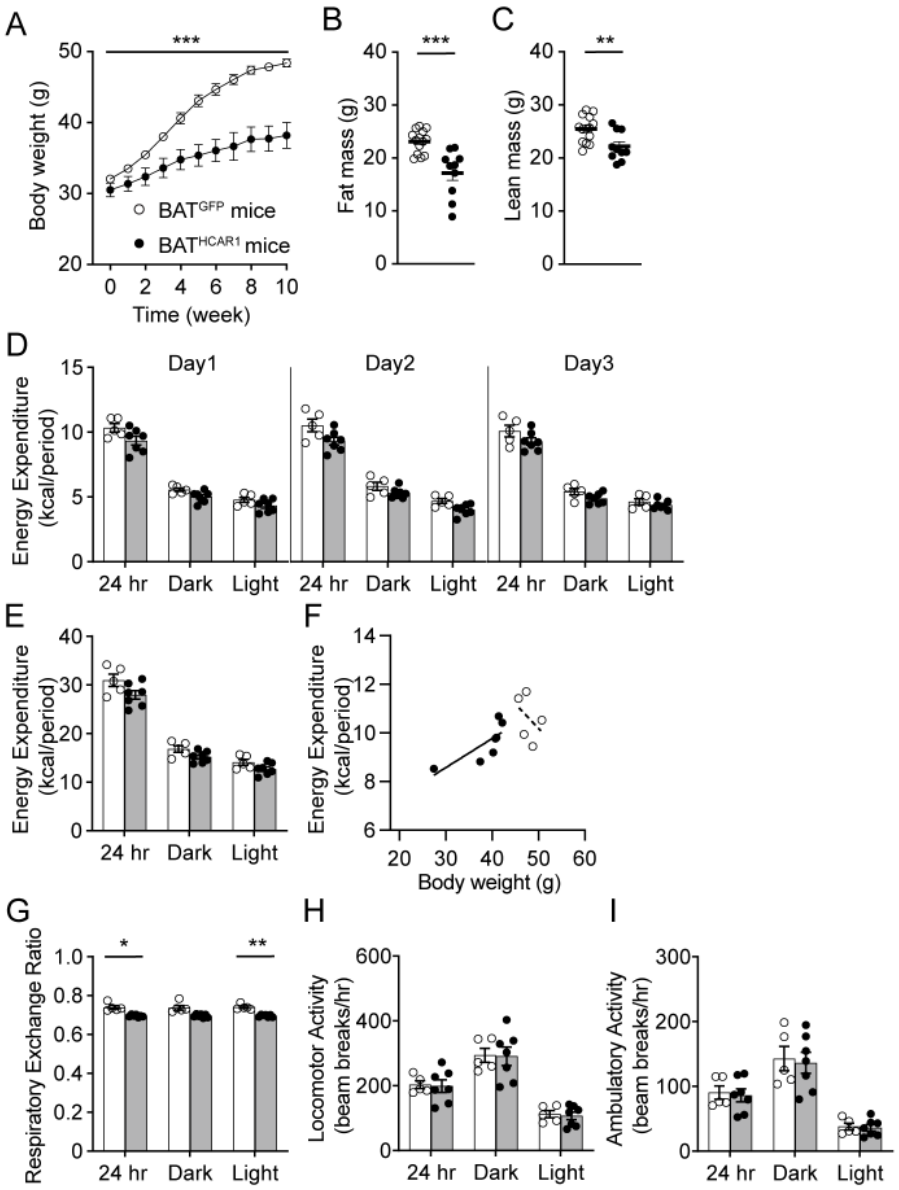

Figure 3

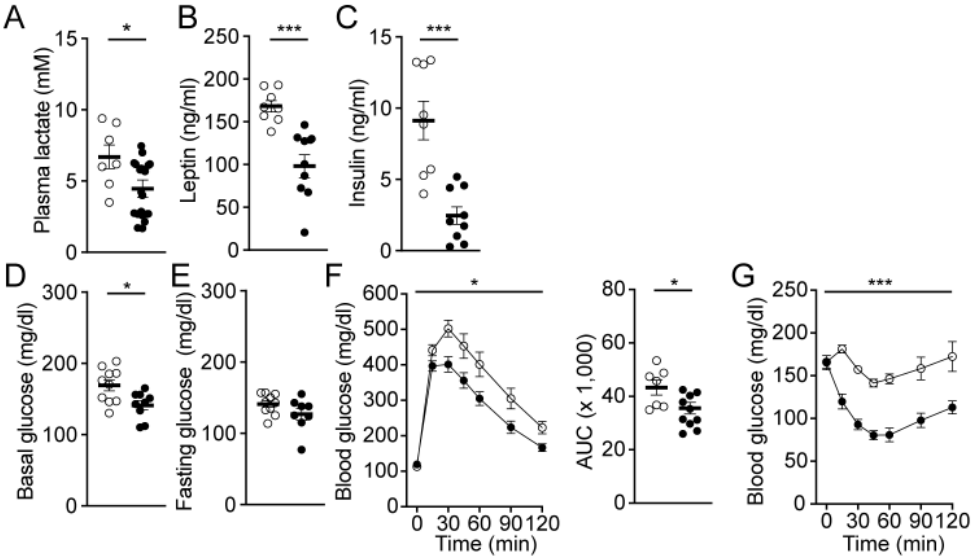

Figure 4

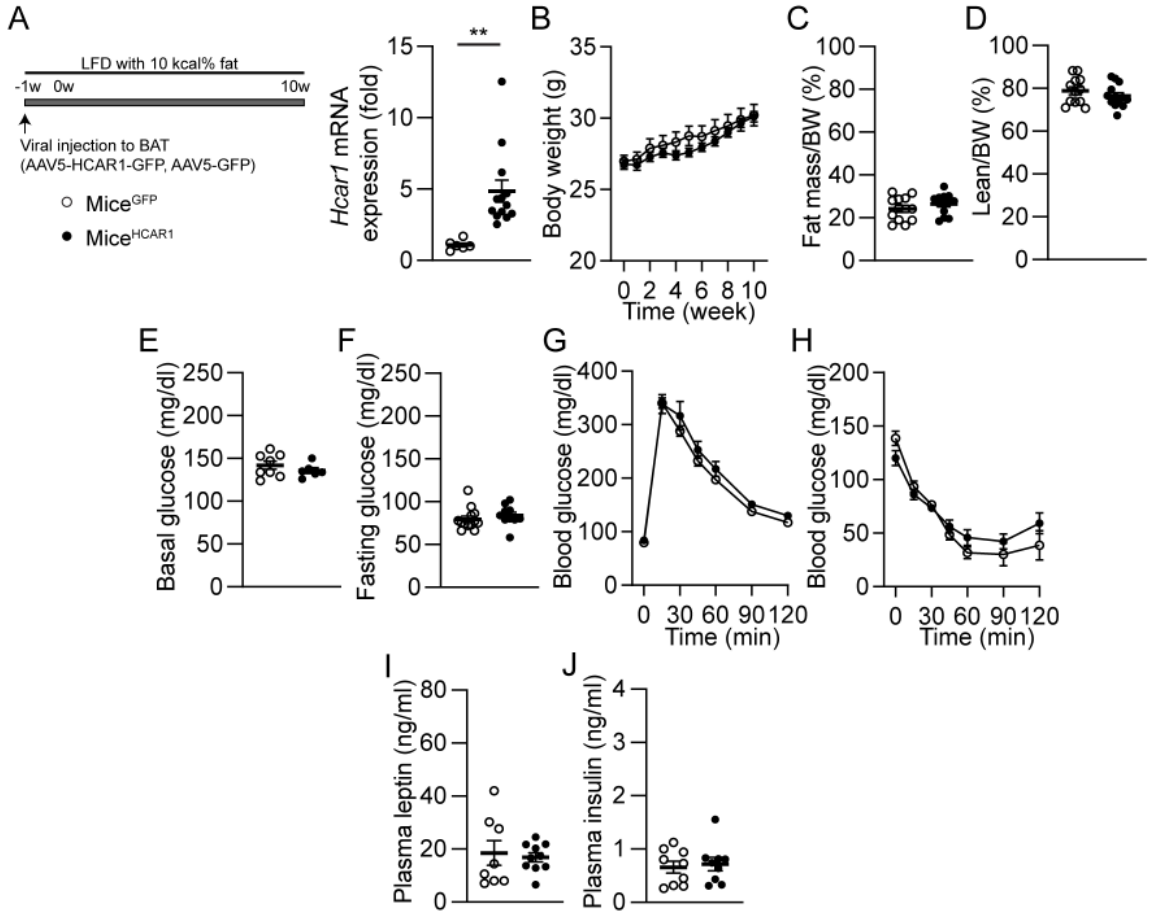

Figure 5

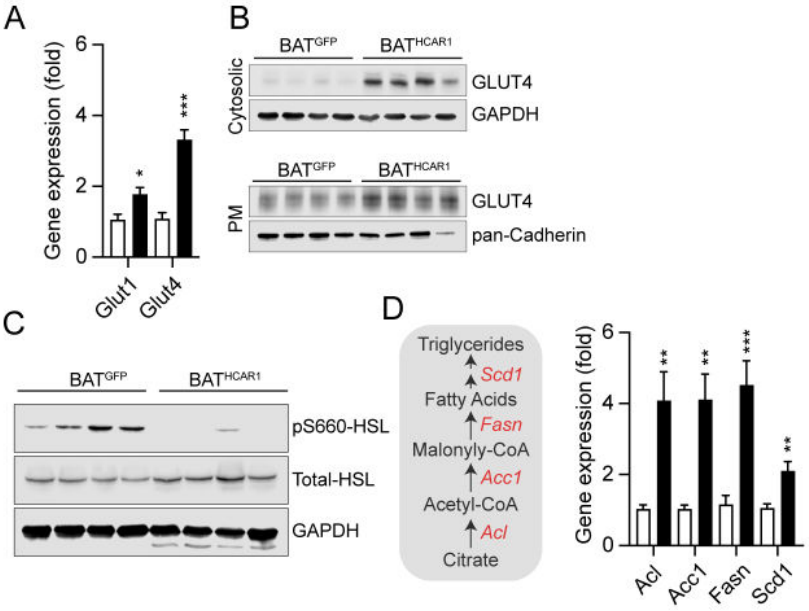

Table 1. List of primer sets for qPCR

Gene	Gene Symbol	NCBI Accession	Forward (5' to 3')	Reverse (5' to 3')
Hydrocarboxylic acid receptor 1	*Hcar1*	NM_175520.5	TGAGGGACTTGTCCACCTGA	CCATTGCTGCCGTAAACAGG
Beta-2 microglobulin	*B2m*	NM_009735.3	TTCAGTCGCGGTCGCTTC	AGGCCGGTCAGTGAGACAAG
Uncoupling protein 1	*Ucp1*	NM_009463.3	CGTTCCAGGACCCGAGTCGCAGA	TCAGCTCTTGTTGCCGGGTTTTG
Proliferative activated receptor, gamma, coactivator 1 alpha	*Ppargc1α*	NM_008904.2	GACAGCTTTCTGGGTGGATT	CGCAGGCTCATTGTTGTACT
Deiodinase, iodothyronine, type II	*Dio2*	NM_010050.4	AATTATGCCTCGGAGAAGACCG	GGCAGTTGCCTAGTGAAAGGT
Solute carrier family 2, member 1	*Slc2a1 (Glut1)*	NM_011400.3	CCATGTATGTGGGAGAGGTG	TTGCCCATGATGGAGTCTAA
Solute carrier family 2, member 4	*Slc2a4 (Glut4)*	NM_009204.2	AAAAGTGCCTGAAACCAGAG	TCACCTCCTGCTCTAAAAGG
ATP citrate lyase	*Acl*	NM_134037.3	CTGGTGTATCGGGACCTGT	CACAAACACTCCTGCTTCCT
Acetyl-Coenzyme A carboxylase alpha	*Acc1*	NM_133360.2	CTCTGCTAGAGCTGCAGGAT	CTGGGAAACTGACACAGGAC
Fatty acid synthase	*Fasn*	NM_007988.3	ACCTCTCCCAGGTGTGTGAC	CCTCCCGTACACTCACTCGT
Stearoyl-Coenzyme A desaturase 1	*Scd1*	NM_009127.4	AGAGAACTGGAGACGGGAGT	GCATCATTAACACCCCGATA